JOURNAL OF GEOPHYSICAL RESEARCH, VOL. 101, NO. C4, PAGES 8759–8773, APRIL 15, 1996

Scales of spatial and temporal variability in the Southern Ocean

Sarah T. Gille
Physical Oceanography Research Division, Scripps Institution of Oceanography, La Jolla California

Kathryn A. Kelly
Department of Physical Oceanography, Woods Hole Oceanographic Institution, Woods Hole Massachusetts

Abstract. Spatial and temporal variability in Geosat altimeter data is used to consider whether the Antarctic Circumpolar Current (ACC) responds on the large scale to global changes in wind forcing or whether its variability is primarily mesoscale. The Geosat data indicate a spatial decorrelation scale of 85 km and a temporal e-folding scale of 34 days. Using these scales to define autocovariance functions, the sea surface height variability is objectively mapped. The resulting maps indicate substantial evidence of mesoscale eddy activity. Over 17-day time intervals, meanders of the Polar Front and Subantarctic Front appear to elongate, break off as rings, and propagate. Statistical analysis of ACC variability from altimeter data is conducted using empirical orthogonal functions (EOFs). The first-mode EOF describes 16% of the variance in total sea surface height across the ACC; reducing the domain into basin scales does not significantly increase the variance represented by the first EOF, suggesting that the scales of motion are relatively short and may be determined by local instability mechanisms rather than larger basin-scale processes. Likewise, neither complex nor extended EOFs indicate statistically significant traveling wave modes.

1. Introduction

Studies of Southern Ocean variability feature two recurring themes. First, because the Antarctic Circumpolar Current (ACC) is zonally connected and driven by large-scale wind patterns, fluctuations in ACC transport are hypothesized to be zonally coherent over global length scales. Second, despite the expected large-scale coherence, the circumpolar ocean is a region of enormous mesoscale eddy variability, as documented by drifter data, current meter records, and altimeter measurements. This study will take advantage of the global mesoscale coverage provided by the Geosat altimeter and surface transport estimates derived from Geosat by *Gille* [1994] to examine whether the strong mesoscale variability can be reconciled with predicted large-scale fluctuations. Ultimately, no evidence for coherent large-scale patterns will emerge from the eddy variability and measurement noise considered in this analysis.

Observational work has characterized the ACC as having short spatial and temporal scales, consistent with the presence of substantial eddy activity. Using historic hydrographic data, *Lutjeharms and Baker* [1980] analyzed the spatial structure of the Southern Ocean; their results indicated rapid spatial decorrelation, with length scales less than 150 km. From satellite-tracked surface drifting buoys, *Patterson* [1985] estimated that the majority of kinetic energy in the Southern Ocean has a timescale of less than 1 month. Current meter results, summarized by *Nowlin and Klinck* [1986], have indicated that most of the energy is associated with timescales of 20–50 days for the surface-intensified, first empirical mode and 7–20 days for the bottom-trapped second empirical mode [*Inoue*, 1985]. Spatial decorrelation length scales for temperature estimated from mooring data were 80–100 km [*Sciremammano et al.*, 1980]. Altimeter measurements also illustrate the strong eddy variability throughout the Southern Ocean and, in particular, show increased levels of eddy variability concentrated along the axis of the ACC [*Shum et al.*, 1990; *Chelton et al.*, 1990; *Gille*, 1994].

In spite of the short spatial scales of eddy variability, in studies of volume transport fluctuations, investigators have usually conjectured that the ACC varies uniformly along its entire circumpolar path. This assumption is made for two reasons. First, existing wind information from ship measurements and from the model of the European Centre for Medium-Range Weather Forecasts (ECMWF) [*van Loon*, 1972; *Large and van Loon*,

Paper number 96JC00203.
0148-0227/96/96JC-00203$05.00

1989] is dominated by global-scale, semiannual fluctuations. If the ACC is driven by these relatively uniform changes in the wind, then its depth-integrated transport might be predicted to vary similarly. Second, regardless of the forcing, the continuous and zonally connected character of the ACC means that transport variations in any given location could drive transport variations everywhere.

Because of the predicted large-scale coherence, most of the past volume transport monitoring of the ACC has been done in Drake Passage, where the flow is confined to a narrow latitude range, and measurements in Drake Passage have been assumed to apply to the entire system. From Drake Passage moorings, *Whitworth and Peterson* [1985] estimated a mean transport of $123 \pm 11 \times 10^6$ m^3 s^{-1}, with deviations as large as 50×10^6 m^3 s^{-1}. *Wearn and Baker* [1980] showed that transport variations estimated from pressure gauges in Drake Passage were significantly correlated with fluctuations in the zonally averaged winds, with a 9-day lag. The reliability of their results has remained uncertain; *Chelton* [1982] argued that the high correlations Wearn and Baker observed could be an artifact of comparing two signals with strong seasonal components. Using surface drifters throughout the entire Southern Ocean from a 1-year interval, *Large and van Loon* [1989] found a substantial annual and semiannual velocity signal, accounting for 30% to 85% of the oceanic variability, depending on the location, but they saw substantial zonal variation and little spatial correlation between low-frequency wind and drifter measurements, in contradiction with the hypothesis of zonally coherent variability. As the ambiguities in observational results indicate, in situ measurements have not provided sufficient information to reconcile our understanding of large-scale forcing in the Southern Ocean with the observed mesoscale eddy variability.

The global synoptic coverage provided by satellite altimeters offers a means to address variability processes more carefully. *Chelton et al.* [1990] used Geosat altimeter measurements at ground track crossover points to examine Southern Ocean variability. Their analysis provided little evidence for circumpolar-scale variability and instead suggested variability might occur on basin-wide or regional scales. However, their method was not designed to capture ACC velocity changes confined to narrow, mesoscale jets; results by *Gille* [1994] indicated that transient eddies not associated with jet meandering accounted for a higher percentage of the variance in the ACC than in the Gulf Stream or the Kuroshio Extension, so that large-scale analyses might be dominated by eddy variability and might not detect coherent transport fluctuations.

This study will use mesoscale analysis techniques to more specifically examine scales of variability in the Southern Ocean. To do this, we take advantage of the collinearly processed Geosat data and the mean sea surface height which has been reconstructed by fitting a meandering Gaussian jet to the altimeter measurements [*Gille*, 1994]. In section 2, length scales and timescales of variability are estimated from data and used to map instantaneous sea surface height. The resulting figures illustrate how the substantial variability appears to be associated with local mesoscale processes, such as meandering and ring formation along the ACC fronts, rather than large-scale fluctuations. In section 3, temporal and spatial scales of surface transport variability will be estimated by computing empirical orthogonal functions. Here surface transport will refer to integrated surface velocity, which is equivalent to the height difference between the northern and southern edges of the circumpolar current; surface transport is not the same as the depth-integrated volume transport, though the two quantities may be correlated, as suggested by the strong vertical coherence of Southern Ocean variability [*Whitworth et al.*, 1991]. One might envision a scenario in which a constant background level of eddies controlled the momentum balance, while ACC transport responded directly and in a globally coherent way to wind forcing. However, the results of this study, discussed in section 4, will instead suggest that mesoscale eddy motions dominate Southern Ocean surface transport variability, and there is little evidence for coherent transport fluctuations. Section 5 summarizes the findings.

2. Scales of Variability

2.1. Time-Varying Sea Surface Height

The autocovariance of sea surface height provides a measure of the cross-correlation of variability at points separated in time and space. If a large region fluctuates in unison, then the autocovariance will be high and will decrease slowly as a function of distance. If spatial fluctuations occur over short distances, then measurements taken at nearby points will be uncorrelated, so that the autocovariance will decrease rapidly with distance. Similarly, the timescales over which the autocovariance decreases indicate the temporal scales of variability of the measured data.

Sea surface height variability data were employed from all 244 ascending and 244 descending collinear ground tracks from the Geosat altimeter. The raw data were initially processed to remove outliers, corrected, and filtered following the procedure outlined by *Gille* [1994] (but the Gaussian jet model discussed by Gille was not employed at this stage). For a 350-km swath centered around the core velocity jets of the ACC, along-track spatial and temporal autocovariances were computed. Functional parameters were then fit to the autocovariance data to define length scales and timescales of variability, as described below.

Stammer and Böning [1992] found that length scales in the ocean varied considerably with latitude but were relatively constant in longitude; careful examination of

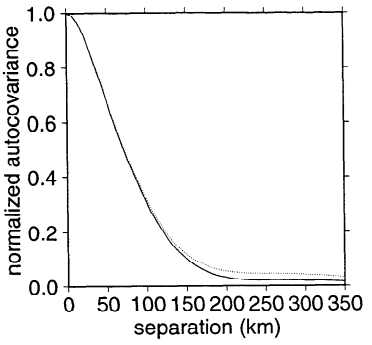

Figure 1. Spatial autocovariance for ascending (solid line) and descending (dotted line) tracks, averaged over all ground tracks and normalized to a maximum amplitude of 1 at 0 lag. Differences between ascending and descending tracks are not statistically significant. Confidence limits increase with large separations, but as the autocovariances represent an average of 40 to 60 passes over the 244 ground tracks, estimated errors are small for all lags.

the autocovariances as a function of longitude in this analysis supports their findings and also suggests that the temporal autocovariance does not vary regionally. Since the latitude of the ACC changes by only about 20°, meridional changes in the autocovariance are not discernible, and any possible variations in the length scales are unlikely to be large enough to effect the objective maps. Therefore no geographic variation is included in the decorrelation functions defined for this study. Figure 1 shows the normalized mean spatial autocovariance for ascending and descending tracks, and Figure 2 shows the normalized mean temporal autocovariance. The negative temporal autocovariance at lags greater than 80 days is an artifact of the finite duration of the time series [*Gille*, 1995].

On the basis of the autocovariances represented in Figures 1 and 2, the correlation function c is assumed to be Gaussian in space and exponential in time:

$$c_{i,j} = D \exp\left[-\frac{\Delta d_{ij}^2}{B^2}\right] \exp\left[-\left|\frac{\Delta t_{ij}}{T}\right|\right] + C\delta_{ij}, \quad (1)$$

where i and j are indices of data being correlated, Δd is the spatial separation between data points, Δt is the time separation, and δ_{ij} is 1 when $i = j$ and 0 otherwise. By least squares fitting (1) to the covariances determined from the data, the amplitude D is estimated to be 0.012 m^2, the length scale B, to be 85 km, and the timescale T, to be 34 days. For measurements from the same satellite pass along a single ground track the zero lag offset C is 0.001 m^2, corresponding to the 0.03-m rms noise assumed for the Geosat altimeter. When different ground tracks or different satellite passes are compared, C is 0.004 m^2, corresponding to 0.065 m rms for instrument noise, orbit error, and residual atmospheric and electromagnetic (EM) bias corrections.

The 34-day timescale is comparable to upper ocean timescales of 20 to 50 days estimated from Drake Passage current meter data [*Inoue*, 1985] and to e-folding scales of 20 to 30 days estimated from Southern Ocean temporal autocorrelation functions plotted by *Minster and Gennero* [1995] in their analysis of ERS 1 altimeter measurements on a 3-day repeat. The 85-km length scale is approximately the same as the diameters of smaller observed rings, which have varied in size from 60 to 200 km [*Bryden*, 1983], and is akin to the spatial decorrelation length scales for temperature found by *Sciremammano et al.* [1980].

The mean sea surface height, objectively mapped by *Gille* [1994], varied more rapidly in the meridional direction than in the zonal direction. However, within measurement constraints, no equivalent anisotropy is identifiable in sea surface height variations. Ascending and descending tracks show similar eddy variability length scales, but do not distinguish the zonal and meridional directions. Since the spatial and temporal scales of eddies are comparable to the track separation in the latitudes of the ACC, adjacent tracks cannot be combined to examine zonal wavenumber spectra in greater detail. In situ measurements in Drake Passage are consistent with the altimeter analyses; although velocity variations are anisotropic, temperature fluctuations, which are a better analog to sea surface height, are isotropic [*Sciremammano et al.*, 1980].

On the basis of the length scales and timescales found in this study, sampling of altimeter data variability is judged to be marginally sufficient to avoid aliasing high-frequency motions. (See the appendix for a full discussion.) Therefore the correlation function (1) is used to objectively map along-track sea surface height anomalies and estimate errors using the technique outlined by *Bretherton et al.* [1976]. The mean sea surface height from *Gille* [1994] is added to the mapped sea surface height anomaly field. Figure 3 shows the resulting instantaneous sea surface height for December 28, 1986. Formal objective mapping errors in the instantaneous

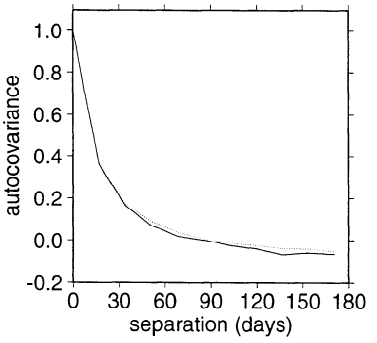

Figure 2. Temporal autocovariance for ascending (solid line) and descending (dotted line) tracks, averaged over all ground tracks and normalized to a maximum amplitude of 1. Differences between ascending and descending tracks are not statistically significant.

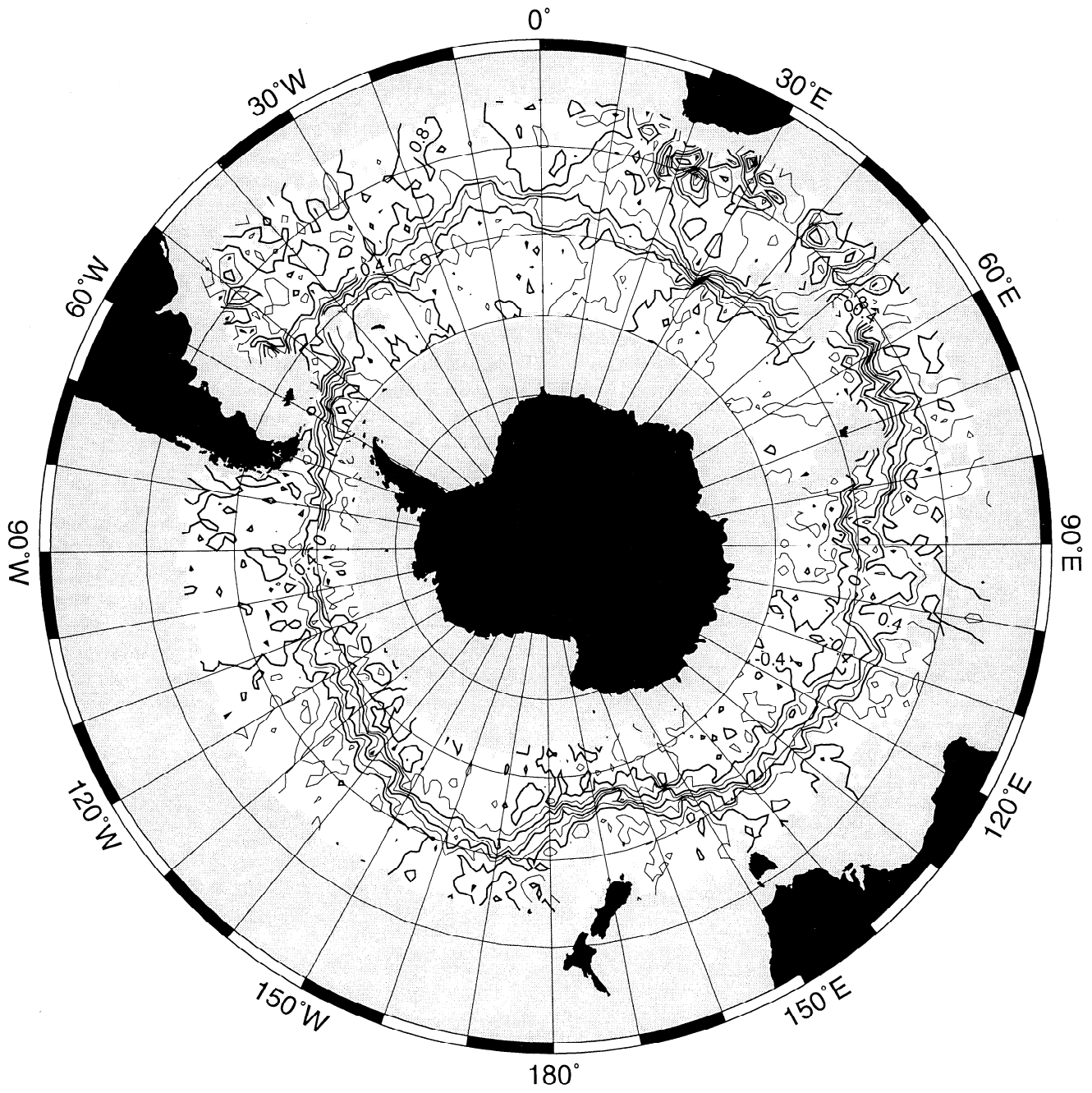

Figure 3. Synoptic map of reconstructed sea surface height for December 28, 1986, with a contour interval of 0.1 m. Regions with no data or height errors greater than 0.07 m are gray, and contours are not shown when the error exceeds 0.12 m. Over most of the region, errors are between 0.05 and 0.07 m; the largest errors are at the edges of the analyzed region, where the least data are available.

sea surface height are estimated between 0.05 and 0.07 m over most of the domain.

2.2. Local Eddy Processes

Objective maps graphically illustrate what the decorrelation length scales represent numerically: dominant variability is associated with mesoscale eddy structures rather than large-scale shifts in the zonal current. To more closely examine this, consider the eddy intense region south of New Zealand. Figure 4 indicates the mean sea surface height for the region reconstructed following the procedure outlined by *Gille* [1994]. Shown superimposed over bathymetry from the ETOPO5 (5-min resolution bathymetric) data, the mean sea surface height is closely steered by bathymetry along the Southeast Indian Ridge, through the Macquarie Ridge complex, and around the Campbell Plateau. In this analysis the ACC is assumed to contain two meander-

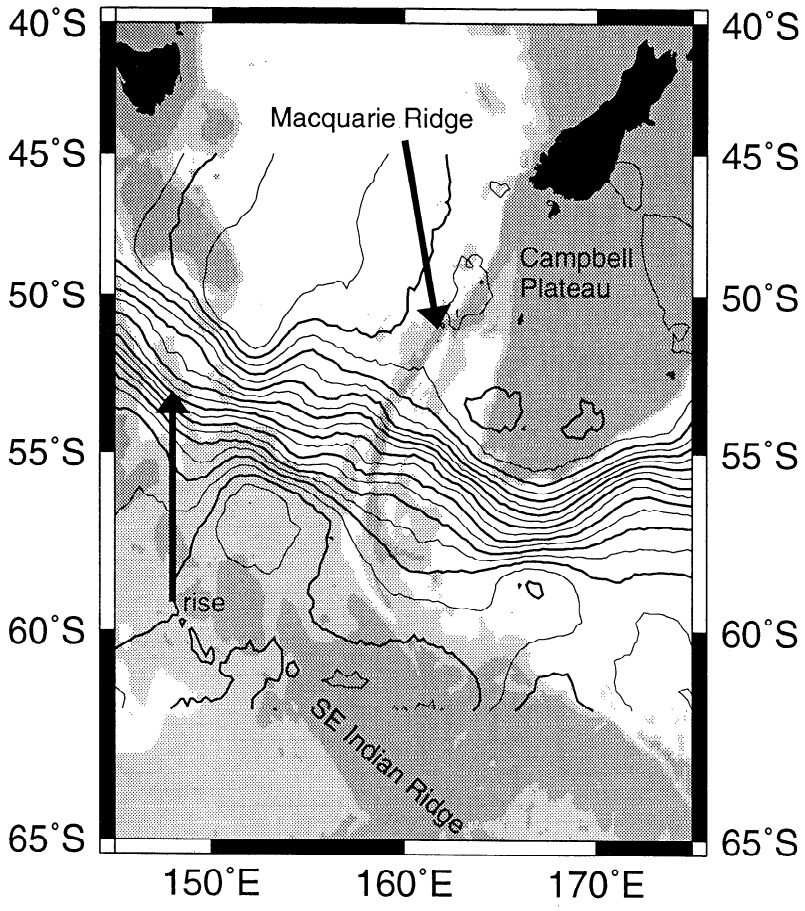

Figure 4. Mean sea surface height south of Australia and New Zealand, reconstructed using the technique described by *Gille* [1994]. Sea surface height is in meters, with a 0.1-m contour interval. Results are superimposed on ETOPO5, 5-min resolution bathymetric data. Dark gray regions are shallower than 3000 m, and light gray regions are shallower than 4000 m.

ing fronts, the Subantarctic Front (SAF) and the Polar Front (PF), roughly separated by the zero height contour. Although the resolution of the mean sea surface height does not sharply distinguish the two fronts, the mean map suggests that the topographic rise at 148°E, 53°S (indicated by an arrow) separates the SAF and the PF. In the Macquarie Ridge complex the SAF passes to the north of Macquarie Island (located around 160°E, 55°S but not resolved by the mapped bathymetry) and the PF to the south.

The rms sea surface height in Figure 5 indicates that the mean flow is concentrated in regions of elevated variance. The variance is greatest south of New Zealand, where the ACC jets are steered around Campbell Plateau, and also appears particularly large just downstream of the two gaps in the Macquarie Ridge system through which the ACC fronts appear to flow.

Instantaneous eddy fields, objectively mapped onto a quarter-degree grid, are added to the mean sea surface height to produce a time sequence (and error map) illustrating eddy processes in the Southern Ocean (Figure 6). The time series indicates two continuous meandering jets which stretch across the domain, superimposed on an energetic background eddy field. Both the SAF and PF meander substantially as they travel southeast from 145°E, 50°S to 165°E, 58°S and then northeast around Campbell Plateau. Nonetheless, rings and ring formation processes are clearly a significant portion of total eddy variability. *Gille* [1994] indicated that meandering accounted for less than half of the rms sea surface height in eddy active regions downstream of topography.

The time sequence shown here, with its numerous ring structures, provides anecdotal evidence to corroborate the statistics. From the first image to the last we see evidence of a meander at 157°E, 57°S (indicated by the bottom box in Figure 6a) gradually elongating, breaking off, and moving away from the Polar Front. Just to the north of that feature, at 157°E, 53°S, a meander on the northern side of the PF (indicated by the top box in Figure 6a) separates from the front to form a coherent ring and finally coalesces into the center of an SAF meander, suggesting a mechanism by which eddy processes may directly transport water masses across the Polar Frontal Zone.

These images provide a qualitative picture of strong

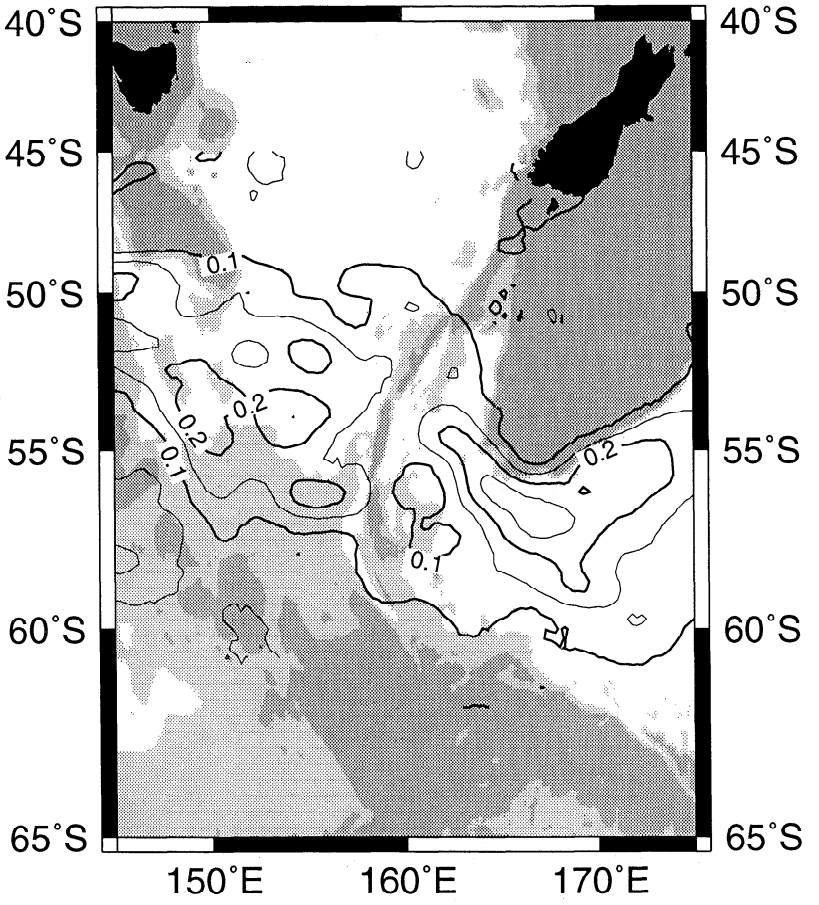

Figure 5. Root-mean-square sea surface height (in meters) south of Australia and New Zealand. The contour interval is 0.05 m.

mesoscale variability without global-scale fluctuations. In the next section, statistical techniques will be used in an attempt to quantify the large-scale variability of the ACC.

3. Seeking Coherence in Variability

3.1. Time Domain Variability

Empirical orthogonal functions (EOFs) [*Davis*, 1976] provide the statistical machinery necessary to assess whether the ACC fluctuates coherently in response to seasonal wind forcing or any other temporally varying effects. In this analysis, EOFs are computed on the variations in total surface transport in the ACC jets as a function of time and longitude, as determined by *Gille* [1994]. The time series of sea surface height difference across the ACC for each of the 488 tracks, at 63 steps in time were Fourier transformed to the frequency domain using a technique which accounts for the data gaps in the time series [*Ferraz-Mello*, 1981]. Ascending and descending tracks were treated as separate data sets because of the complications associated with merging information from intersecting tracks when the latitude of the current varies substantially as a function of longitude. On the global scale the results for ascending and descending data are similar; EOF results will only be plotted for descending tracks since the descending data suffer from fewer gaps.

Figure 7 shows wavenumber and frequency spectra for all of the surface transport estimates. A boxcar-hanning window was applied to exclude all but the lowest 15 frequencies, corresponding to a maximum of about five cycles per year, where the spectrum is red, and the data were inverse transformed to produce a complete time-space series of sea surface height differences. Although the wavenumber spectrum is somewhat white, with a peak around 40 cycles per 360°, it indicates that the greatest energy is at low wavenumbers. The data were therefore spatially filtered, retaining roughly the lowest 20 zonal wavenumbers, where wavenumber 20 corresponds to about 18° longitude or 1000 km, in order to examine large-scale phenomena.

EOFs were computed using a singular value decomposition [*Kelly*, 1988]. In the results presented, each EOF mode represents coherent changes in sea surface height as a function of time; the amplitude of the mode varies spatially, but the phase is globally constant. The first-mode EOF captures the largest percentage of the variance, which can be explained by coherent variations

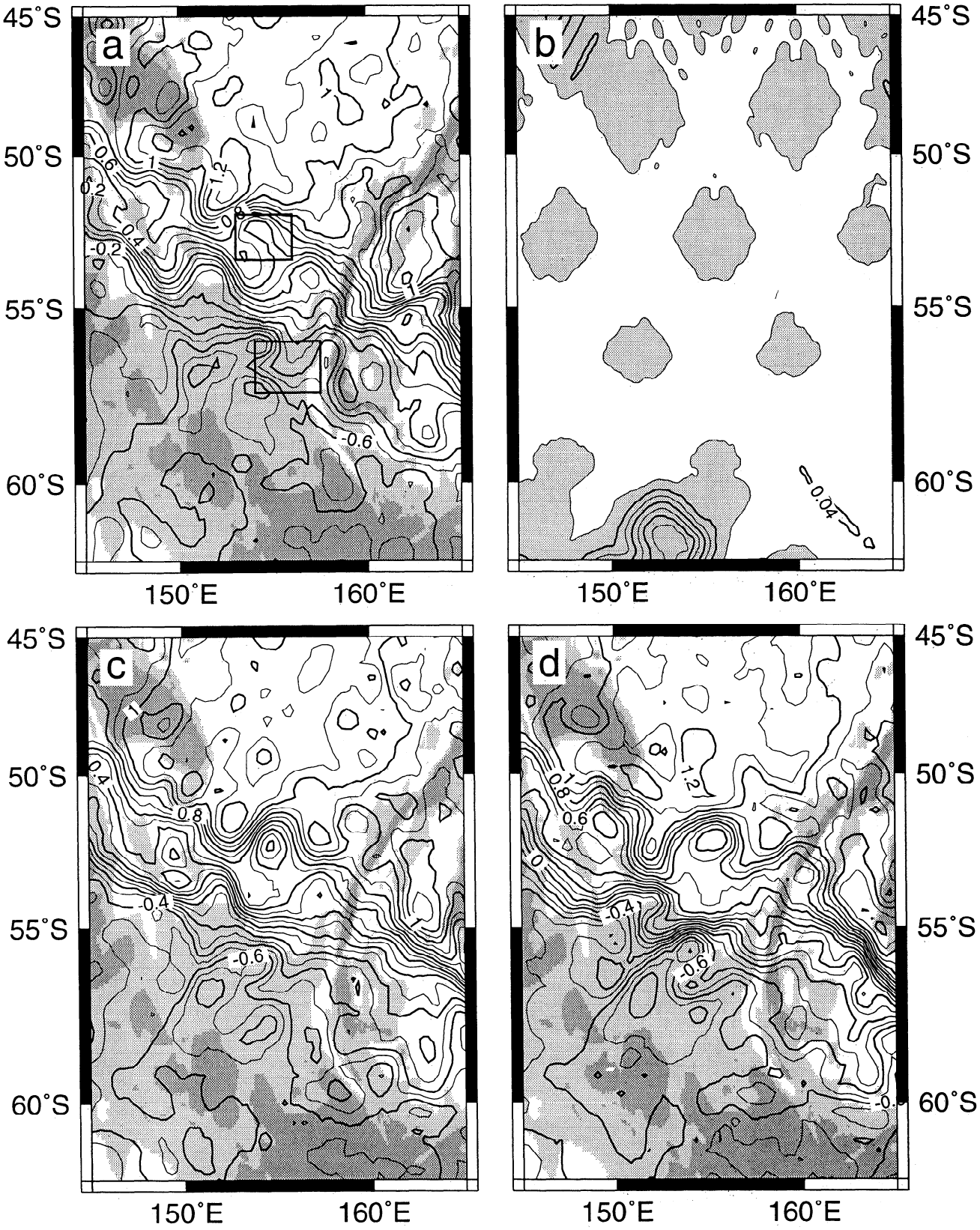

Figure 6. (a) Instantaneous sea surface height south of Australia and New Zealand for April 9, 1987, reconstructed by adding the mean field in Figure 4 to the objectively mapped instantaneous height. Sea surface height is in meters and is contoured with a 0.10-m contour interval. Results are superimposed on ETOPO5, 5-min resolution bathymetric data. Dark gray regions are shallower than 3000 m, and light gray regions are shallower than 4000 m. (b) Error map for instantaneous sea surface height shown in Figure 6a. Most of the region has errors between 0.05 and 0.07 m; gray regions indicate errors greater than 0.06 m. The contour interval is 0.02 m. (c) Instantaneous sea surface height for April 26, 1987. (d) Instantaneous sea surface height for May 13, 1987.

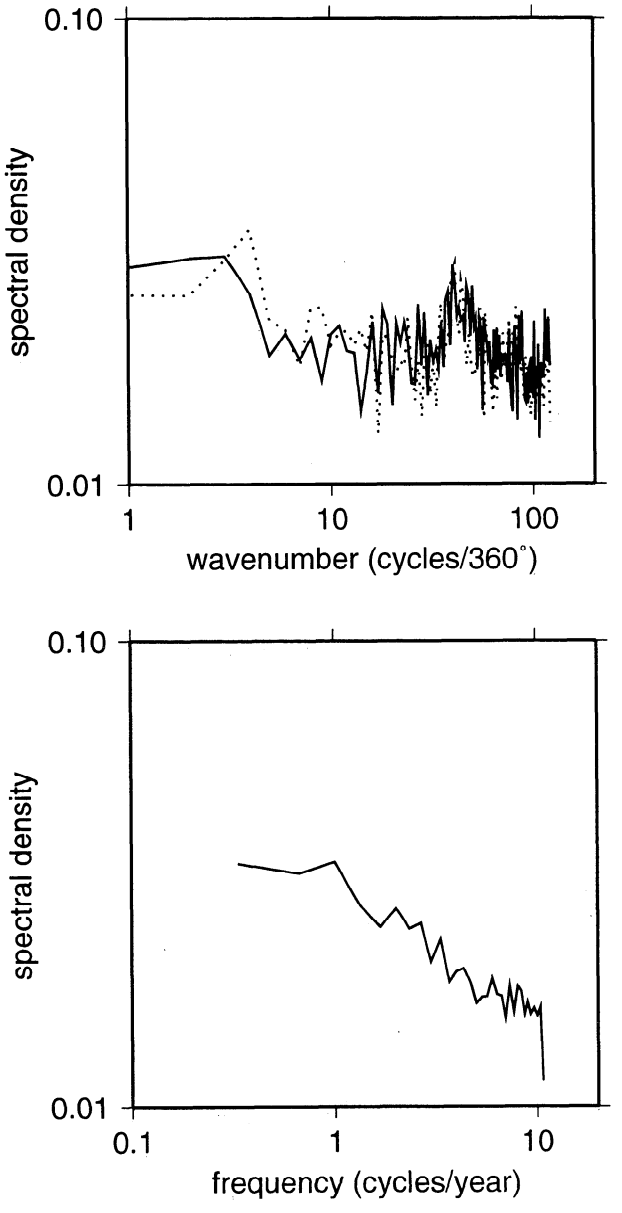

Figure 7. (top) Wavenumber spectrum for surface transport variability for ascending and descending track data combined. Solid line represents westward propagating features, and dashed line represents eastward propagating features. (bottom) Frequency spectrum for surface transport variability for ascending and descending track data combined. Values shown represent the power spectral density (in square meters).

in surface transport, and the remaining EOFs are sorted according to decreasing variance represented. Thus, if the dominant fluctuations in ACC transport were globally coherent and in phase, as *Wearn and Baker* [1980] suggested, then at all longitudes the first-mode EOF would have roughly the same amplitude. Conversely, if the leading mode EOFs explain little of the variance and are not global in structure, as these results will indicate, then we conclude that the dominant fluctuations in ACC transport occur on smaller spatial scales.

3.1.1. EOFs for the full Southern Ocean. The first EOF for the entire Southern Ocean domain accounts for 16.5% of the variance in descending track data and 16.6% in ascending track data. The spatial structure of the mode does not show large-scale structures, and the fraction of variance explained as a function of longitude (Figure 8) indicates that most of the mode's effect is concentrated in a few locations.

None of the higher-order modes is any more suggestive of larger-scale structure in the variability. In the time domain (Figure 9) the first-mode EOF fluctuates on roughly a semiannual (180 day) timescale, but without a single, well-defined frequency. Higher-order temporal modes do not clearly correspond to annual or semiannual timescales, which might be interpreted as a response to wind forcing. The magnitude and timescale of first mode EOF fluctuations are comparable to the variations seen by *Wearn and Baker* [1980], suggesting that the Drake Passage variability measured by pressure gauges may be typical of the full Southern Ocean, even if the overall response is not coherent.

Significance levels were tested using rule N outlined by *Preisendorfer* [1988]. This is a Monte Carlo tech-

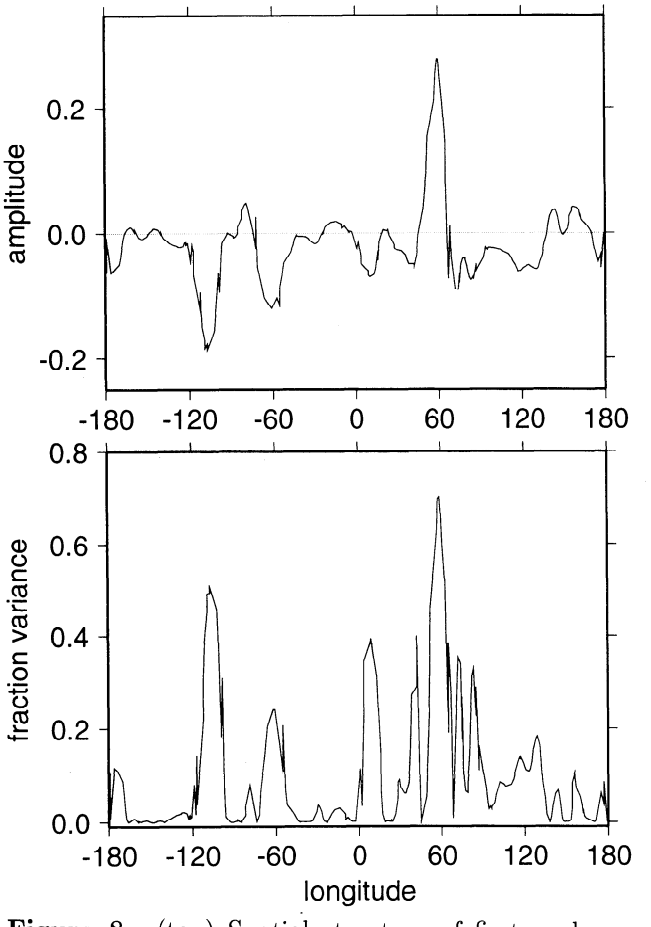

Figure 8. (top) Spatial structure of first-mode empirical orthogonal function (EOF) for all descending track data (in meters). (bottom) Fraction of variance explained by the first-mode EOF as a function of longitude.

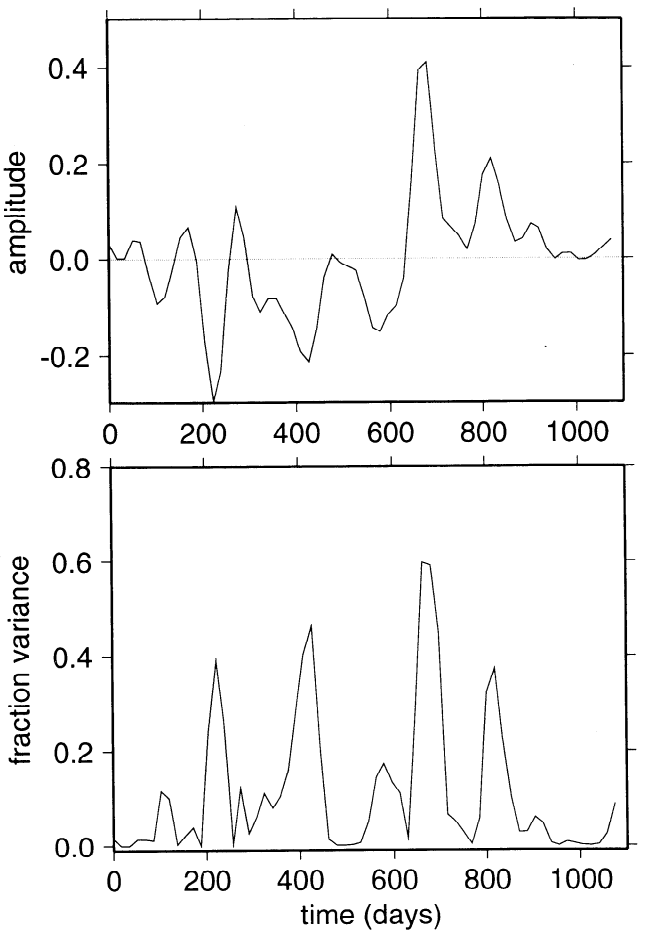

Figure 9. (top) Temporal structure of first-mode EOF for all descending track data (in meters). (bottom) Fraction of variance explained by the first-mode EOF as a function of time.

nique, in which EOFs are computed for 100 sets of white noise which have been filtered and treated in the same way as the raw data, producing 100 sets of eigenvalues l_j, where j goes from 1 to n, the number of data eigenvectors. By numerically sorting the 100 eigenvalues at each j and selecting the 5th and 95th values, 90% significance bounds are determined; those eigenvalues which exceed the upper limit are interpreted to represent eigenmodes which are statistically different from white noise.

On the basis of rule N, the first five modes of the Southern Ocean EOF analysis are statistically significant (Figure 10). Together, these five modes account for 57% of the variance of descending tracks and 56% for ascending tracks. Thus over 40% of the variance is not described by coherent variability. The low percentages of variability represented by the first few EOFs are comparable to the results found by *Chelton et al.* [1990], who showed that the first EOF accounted for only 15% of the variance of filtered height variability at Geosat crossover points in the Southern Ocean. The close quantitative match with Chelton's results suggests that the EOF modes may capture representative processes in the Southern Ocean surface circulation. These results imply that dominant Southern Ocean variability is not global in scale.

3.1.2. Basin scale and regional EOFs. If the Southern Ocean does not undergo system-wide fluctuations, it may still be coherent on a basin scale, with regional flow patterns broken up by the topographic features which separate it into basins and which are associated with substantial eddy variability. Indeed, separating the flow into basins shows a substantial increase in the percentage of the variance accounted for by the first few EOFs. *Chelton et al.* [1990] found that first-mode EOFs explained 26%, 21%, and 22% of the variability in the Atlantic, Indian, and Pacific sectors, respectively. In this analysis a number of different basin divisions of varying sizes were examined using both continental margins and bathymetric features to define the basin limits. The first-mode EOFs account for between 20% and 35% of the variability, depending on the basin considered and the precise boundaries of the basin, as indicated in Table 1. Substantial differences between ascending and descending tracks are not surprising because of differences in the orientation of the tracks and the number of data points available in each ocean basin. Since the percentage variance explained in each basin was very small, a number of subbasin regions were also considered. Regardless of basin size and track orientation, rule N tests indicate that a maximum of two modes are statistically significant at the 90% level, as illustrated for several examples in Figure 11. Overall, these results are consistent with Chelton *et al.*'s [1990] results and suggest that Southern Ocean variability may be better described by basin-scale motions rather than global fluctuations.

The full interpretation of these modes, however, can be deceptive. In any statistical system, reducing the number of degrees of freedom (in this case, the number of sea surface height locations considered) will necessar-

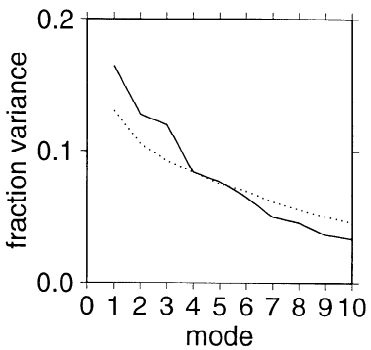

Figure 10. Percentage of variance explained by the first 10 EOF modes for descending track data (solid line), and rule N test values indicating the 90% significance limits for EOFs computed on pure white noise (dotted line). Only EOF modes exceeding this significance limit are judged to be statistically meaningful. See text.

Table 1. Percentage Variance Explained by First-Mode Empirical Orthogonal Function for Basin-Scale Regions of the Southern Ocean

Region	O[a]	Percent Variance	N Modes	N Modes With Reduced Degrees of Freedom
Southern Ocean	a	16.6	5	
	d	16.5	5	
Atlantic Ocean				
52°W–70°E	a	26.3	2	0
	d	38.4	2	1
70°W–25°E	a	35.0	2	1
	d	36.6	2	1
Indian Ocean				
70°E–170°E	a	26.4	0	0
	d	33.1	1	1
25°E–170°E	a	21.4	0	0
	d	29.0	2	2
Pacific Ocean				
170°E–52°W	a	23.4	1	0
	d	25.5	2	1
170°E–70°W	a	19.5	2[b]	0
	d	30.4	1	1
Central Pacific				
170°W–110°W	a	34.2	0	0
	d	34.5	1	0
Central Indian				
42°E–101°E	a	31.6	0	0
	d	49.5	1	1
Eastern Atlantic				
10°W–50°E	a	33.0	0	0
	d	26.6	0	0

Ocean basins are defined first by geographic features, Drake Passage, Kerguelen Island, and Campbell Plateau, and second by continental divisions. "N modes" indicates the number of EOF modes estimated to be significant at the 90% level based on an N test (described in text). "Reduced Degrees of Freedom" indicates the number of modes estimated to show a statistically significant increase from the basin-scale values (see text).

[a]Orientation of ground tracks is either ascending (a) or descending (d).

[b]The first mode is not significant, but the second and third are.

ily increase the magnitudes of some of the eigenvalues. When a smaller region is considered, we must ask not simply whether the percent variance described by the first few modes increases, but more specifically, whether it increases by a statistically significant margin, given the reduction in the degrees of freedom.

To test precisely this issue, synthetic data were created for the Southern Ocean as follows: Gaussian white noise was filtered, subsampled, and decomposed to compute EOFs in the same way as the original sea surface height measurements. The eigenvectors determined from white noise were retained, but eigenvalues were fixed to correspond to the eigenvalues of the filtered data for the entire Southern Ocean. Thus the relative importance of the modes in the synthetic data is the same as in the real data, but the spatial structure of the modes is random and has no link to physical features within the ocean. When the number of samples used was reduced to look at basin-scale variability, the ensemble of eigenvalues for the synthetic data was sorted and interpreted to indicate 90% significance levels. This procedure is analogous to the more conventional rule N outlined previously. Only if the real EOFs exceed the 90% limits can they be interpreted as indicating significant basin-scale motions. The results of this test are indicated as dashed lines in Figure 11. Although rule N indicated that as many as two EOFs were statistically significant, when we took into account the reduction in degrees of freedom, these EOF modes were only marginally significant, and often, no modes were significantly different from their global-scale equivalents. In other words, the apparent increase in the variance explained by the first-mode EOF was largely an artifact of reducing the size of the data set. These tests suggest that Southern Ocean variability is not characterized by large single modes sloshing up and down, either on the global or basin scale.

The geographic distribution of the variance explained by the EOFs supports this conjecture. The first-mode EOF for the entire Southern Ocean (Figure 8) explains almost all of the variance in isolated 1000-km-long regions typically associated with topography, such as the Eltanin-Udintsev Fracture Zone in the middle of the Pacific (130°W). Since the spatial filter eliminates variability on spatial scales less than about 1000 km, the dominant EOF modes cannot capture mesoscale features, but they are clearly not associated with basin or global-scale variability. Figure 12 shows that even when basin-scale and smaller regions of the Southern Ocean are considered, the first-mode EOF does not describe basin-wide variability; instead, its effect is confined to smaller regions. Places where the first-mode EOF describes most of the variance are associated with topographic features and have greater eddy variability. For the regions shown in Figure 12, 60°E in the Atlantic is downstream of the Crozet Plateau, and 110°W in the Pacific is downstream of the Eltanin-Udintsev Fracture Zone. While variance-weighted EOFs have a slightly different structure, they also indicate no basin-scale coherence and suggest that variability occurs on length scales of no more than 1000 km. Thus all evidence from this time domain EOF analysis suggests that the Southern Ocean does not show a large-scale coherent response to wind forcing.

3.2. Propagating Variability

Since surface transport in the Southern Ocean does not indicate a spatially stationary coherent response, we might predict that transport fluctuations instead propagate along the length of the ACC in the form of traveling waves. The frequency-wavenumber spectrum

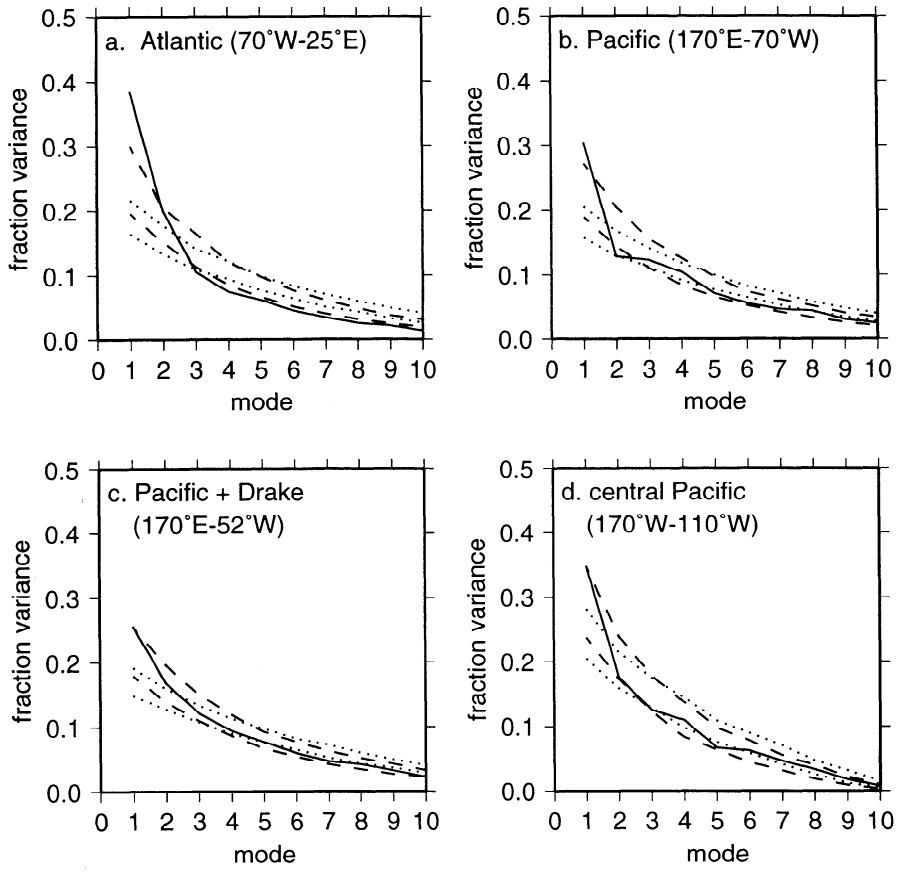

Figure 11. Fraction of variance explained by the first 10 EOFs for the following four regions in the Southern Ocean (solid lines): (a) Atlantic Ocean defined by bathymetry from Drake Passage to Kerguelen Island (70°W–25°E), (b) Pacific Ocean defined by continents (170°E–70°W), (c) Pacific Ocean defined by bathymetry from Campbell Plateau through Drake Passage (170°E–52°W), and (d) central Pacific Ocean (170°W–110°W). Significance levels are determined from N tests performed on filtered white noise (dotted lines) and the relative significance of reducing the number of degrees of freedom (dashed lines).

shown in Figure 13 indicates a statistically significant peak at the annual frequency with increased energy at 0 wavenumber, corresponding to no propagation, and at the wavenumber corresponding to three cycles per 360° propagating westward. The next largest signal propagates eastward with a frequency of 0.33 cycles per year and wavenumber of 3 cycles per 360°.

Although the spectrum appears to indicate strong propagating waves, a nonlinear least squares fit of the data to a traveling wave mode did not explain a significant percentage of the variance. As the broad energy peaks in the spectrum would suggest, no single frequency and wavenumber captures a significant portion of the total variance.

Time domain EOFs do not capture the propagating variability indicated in the frequency-wavenumber spectrum, but complex EOFs [*Barnett*, 1983] and extended EOFs [*Weare and Nasstrom*, 1982; *Graham et al.*, 1987] both provide means to search for dominant traveling wave modes. The first four extended EOF modes and the first two complex EOF modes were statistically significant, and in both cases the significant modes explained 41% of the total variance. However, neither complex EOFs nor extended EOFs exposed any statistically significant traveling wave modes; in both analyses, evidence for both eastward and westward propagation appeared in isolated regions, but no globally coherent structures emerged. As in the global time domain EOF analysis, the fraction of variance explained by the first-mode complex or extended EOF varied substantially with geographic location, suggesting no large-scale coherent behavior above the noise.

4. Discussion: Interpreting Incoherence

These considerations of Southern Ocean surface height fluctuations using EOFs suggest that the dominant scales of variability range from mesoscale to 1000-km scale and that large-scale motions do not clearly propagate through the system. The results are generally consistent with in situ surface observations. *Large and van Loon*'s [1989] analysis of surface drifter veloc-

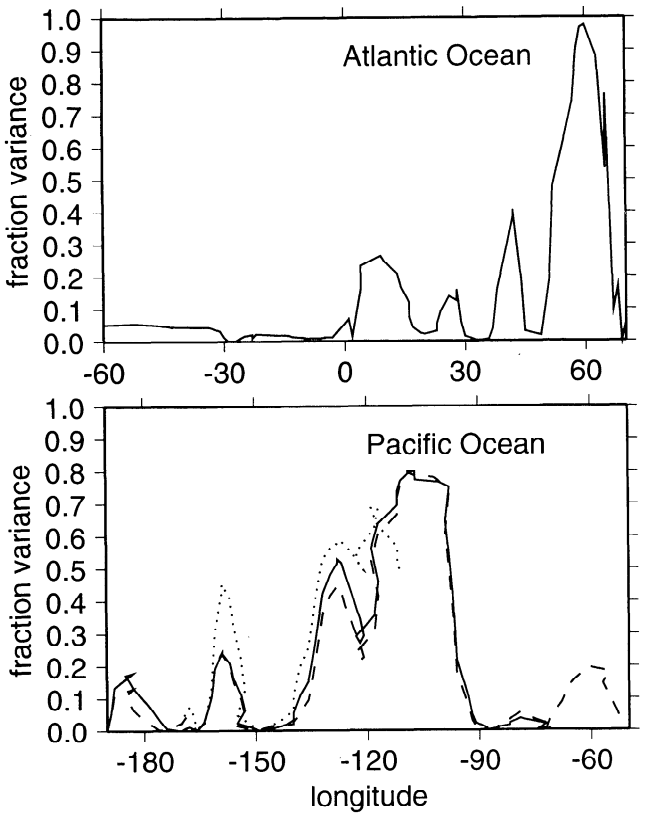

Figure 12. Fraction of variance explained by first EOF as a function of longitude for four regions in the Southern Ocean: (top) Atlantic Ocean defined by bathymetry from Drake Passage to Kerguelen Island (70°W–25°E), and (bottom) Pacific Ocean defined by continents (170°E–70°W) (solid line), Pacific Ocean defined by bathymetry from Campbell Plateau through Drake Passage (dashed line), and central Pacific Ocean (170°W–110°W) (dotted line). Results indicate no clear basin-wide structure.

ities and ECMWF winds indicated that both vary on regional rather than global scales and that the drifters, while similar in phase to the winds at the semiannual harmonic, are dominated by lower-frequency variability than the winds.

Several mechanisms may account for the observed lack of coherence in variability. First, despite well-known observations emphasizing the semiannual cycle in the winds over the Southern Ocean [*van Loon*, 1972], enormous uncertainties remain in the general structure of the fields south of 30°S. The ECMWF model provided the best wind estimates for the Geosat time period, but in a detailed comparison with 1978 scatterometer data, *Mestas-Nuñez et al.* [1994] concluded that ECMWF wind fields were highly suspect over the core of the ACC. ECMWF winds indicate high interannual variability over the major wind belts, although in the ACC the dominant fluctuations occur on annual and semiannual timescales and are global in scale. The results of Mestas-Nuñez et al. suggest that the actual winds may vary much more substantially and on a broader range of scales than the ECMWF fields indicate.

Other measurements also underscore the lack of a strong seasonal cycle in the southern hemisphere. While the work in this paper has examined surface transport estimates, *Stammer and Wunsch* [1994] examined the global sea surface height variability as measured by the TOPEX/POSEIDON altimeter. They found that the amplitude of seasonal sea surface height fluctuations was much smaller in the southern hemisphere than in the northern hemisphere. Stammer and Wunsch interpreted their results based on *Gill and Niiler*'s [1973] work, estimating that most of the seasonal sea surface height variability is due to atmospheric pressure loading and to steric changes in the upper ocean, which they attributed largely to temperature fluctuations rather than salinity changes. Thus the small seasonal signal in the Southern Ocean implies that the system does not experience strong periodic buoyancy forcing and that sea surface temperature does not undergo a large annual

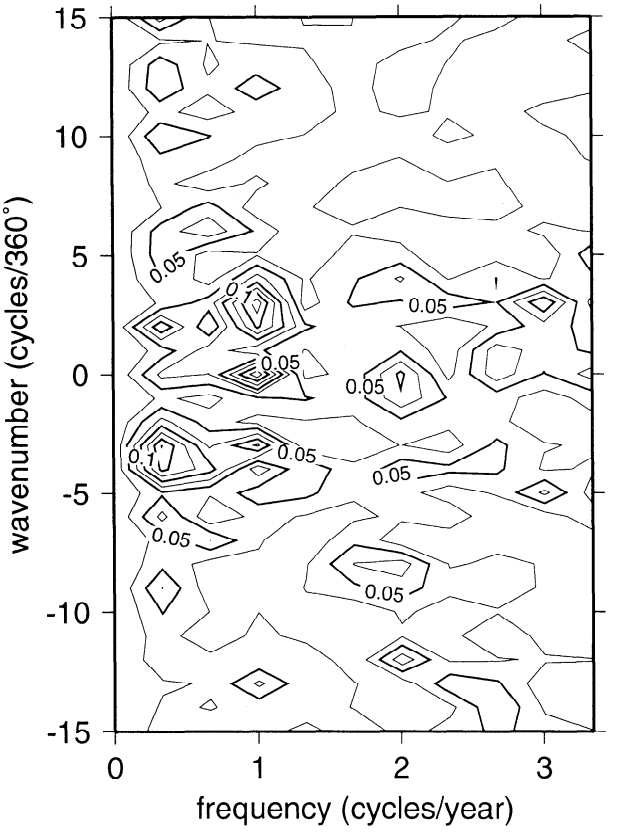

Figure 13. Frequency-wavenumber spectrum for surface transport variability for ascending and descending track data combined. Values shown represent the power spectral density (in square meters). The mean signal as a function of time is removed, so that there is no energy at zero frequency. The peak amplitude has an annual frequency and a wavenumber of +3 cycles per 360° with westward propagation. Amplitudes exceeding 0.05 m^2 (those enclosed by bold lines) are statistically significant at the 95% level based on Monte Carlo results taking into account irregularities in the data sampling.

cycle. Correspondingly, regional processes not associated with global-scale buoyancy forcing may provide the dominant forcing of the Southern Ocean.

Additional factors may prevent the ACC from responding in a globally coherent fashion. Along its convoluted circumpolar path the ACC passes over numerous topographic features which generate form stress, removing momentum input by surface winds. These ridges are associated with substantial mesoscale eddy activity and instability processes which may break up the flow of the ACC and interrupt any large-scale coherent structures. Although numerical model results indicate that form stress occurs predominantly at three major topographic features [*Gille*, 1995], the lack of large-scale coherent oceanic response, even on basin scales, suggests that many more topographic features could be sources of form drag.

Finally, limitations in the altimeter measurements may conceal the oceanic response to wind forcing. First, the mesoscale analysis technique used in this study captures variability in the jets but does not measure any possible response to wind forcing on a broader meridional scale. However, since most of the ACC transport is contained within the narrow jets and the large-scale analysis by *Chelton et al.* [1990] did not indicate globally coherent response, the mesoscale analysis appears unlikely to be a major limitation. Second, the altimeter measures fluctuations in surface transport but is unable to consider how the baroclinic structure of the flow may change with varying wind forcing. Depending on stratification conditions, the rate at which the ACC spins up will differ, so that the flow may deepen in response to wind forcing, increasing total transport without substantially changing surface transport. Southern Ocean observations have not provided a clear picture of the vertical structure of ACC variability. Pressure gauge measurements in Drake Passage suggested that transport fluctuations are largely barotropic [*Whitworth and Peterson*, 1985]; however, *Vassie et al.* [1994b] argued that the annual cycle measured by pressure gauges at Amsterdam and Kerguelen Islands could be partly due to baroclinic changes not seen by the altimeter. Newer pressure gauge and wind measurements will permit continued study. (More recent work with TOPEX/POSEIDON data and improved tidal models has shown close agreement between the Amsterdam Island pressure gauge and altimeter measurements [*Park and Gambéroni*, 1994], which might suggest that baroclinic effects may not be a significant factor in the annual variability.) Preliminary analyses of bottom pressure recorder measurements [*Whitworth and Pillsbury*, 1994; *Vassie et al.* 1994a] show coherence on timescales longer than 50–100 days for transport fluctuations through Drake Passage and the Africa to Antarctica choke point (T. Whitworth, personal communication, 1995). In addition, on longer timescales, W. White and R. Peterson (personal communication, 1995), using a 13-year times series of highly filtered Southern Ocean sea surface temperature, found evidence for a wave propagating around the ACC with a 4- to 5-year period. A low-frequency signal of this nature would not be resolved by the 2.5-year Geosat record.

Ultimately, more detailed observations may be necessary to determine whether substantial spatio-temporal variability in the wind field, topographic forcing, or baroclinic fluctuations account for the lack of coherent structure in this analysis of ACC surface transport. Forthcoming scatterometer measurements of surface winds and ongoing TOPEX/POSEIDON altimeter measurements will undoubtedly provide some illumination.

5. Summary

This work has examined the length scales and timescales of variability and the coherence of fluctuations in the Southern Ocean. Sea surface height variance maps indicate that the Southern Ocean is a region of intense eddy activity, and the decorrelation scales emphasize that much of this variability appears to occur on scales less than 1000 km. Spatial decorrelation scales are relatively short, about 85 km, and timescales are about 34 days. Both of these are marginally well resolved by the Geosat altimeter, but current meter data and analyses of ERS 1 altimeter data from a 3-day repeat orbit have suggested that the Geosat sampling should alias little energy into the sampled frequency-wavenumber space [*Minster and Gennero*, 1995].

The spatial and temporal information defines correlation functions which were used to objectively map instantaneous sea surface height. The maps illustrate the predominance of mesoscale processes in the Southern Ocean. In the region south of New Zealand a series of maps shows a ring forming from a jet meander and breaking away from the Polar Front. Such processes appear more common in eddy intense regions associated with major topographic features and may be a major means by which water mass properties are transported across the ACC, as recent dynamical studies have suggested [e.g., *Johnson and Bryden*, 1989; *Marshall et al.*, 1993].

While eddy processes clearly dominate the sea surface height variability, past studies have predicted that the entire Southern Ocean transport should respond to large-scale variations in the wind forcing. Empirical orthogonal functions computed for the time-varying surface transport suggest no coherent fluctuations on global or basin scales. Coherent variability appears confined to relatively small regions of no more than 1000-km length. This suggests that fluctuations in the wind may be dissipated locally, where they directly influence the surface flow, rather than acting to accelerate ACC surface transport globally. Likewise, frequency domain EOFs indicate no statistically significant traveling wave modes, although the reduced number of degrees of freedom makes detailed analysis difficult.

Appendix : Aliasing Due to Altimeter Sampling Patterns

The Geosat altimeter's 17-day sampling means that variability at frequencies higher than the Nyquist frequency (1 cycle/34 days) may be aliased into the measured signal. While the basic collinear analysis used to treat individual satellite tracks does not introduce substantial aliasing problems (aside from energy at 17-day intervals aliasing into the mean), aliasing is a consideration when adjacent tracks are merged or the data are analyzed as a time series. Since the decorrelation timescale estimated in this study is 34 days, we do not predict substantial variability will be aliased into the measured signal. For Geosat measurements the M_2 tidal alias is of greatest concern since it is nearly indistinguishable from the annual signal. *Jacobs et al.* [1992] took advantage of the tidal alias and least squares fit its phase and amplitude, which varied between 0.01 and 0.05 m in the Southern Ocean. Errors of this magnitude fall well within the error bars of the time dependent signal, but the example of the M_2 tide is indicative of the types of errors that might affect the data interpretation. To examine other frequency ranges that may alias energy, we considered the spectra of pressure measurements from current meters deployed in the Southern Ocean [*Bottero et al.*, 1981]; these suggest that the aliased high-frequency signal is substantially weaker than the sampled signal [*Gille*, 1995]. High-frequency altimeter measurements support this interpretation: *Minster and Gennero* [1995] performed a detailed analysis using ERS 1 altimeter data on a 3-day repeat orbit; their results indicated that only 10 or 15% of the sea surface height variance is not resolved by Geosat.

Spatial aliasing is more difficult to assess. The decorrelation length scale of 85 km is substantially longer than the 7-km along-track sampling interval but very close to the between-track spacing, which varies with latitude from 75 to 125 km. Thus, while the along-track spacing of 7 km is more than sufficient to sample the observed horizontal variability, the spatio-temporal aliasing in large regions poses more difficult problems which are not easily addressed through a simple analysis of historic data sets. *Wunsch* [1989] found that uncertainties in amplitudes of Fourier components for one 17-day period could exceed 50%, but he did not consider time periods longer than 17 days or spatial scales shorter than 6°, which might be more relevant for the mesoscale methods used in this study. More thorough analysis using the strategies outlined by *Wunsch* [1989] and taking advantage of the sampling patterns from newer altimeters should ultimately help to quantify likely spatial sample aliasing.

Acknowledgments. We thank T. Joyce, M. McCartney, and J. Toole for helpful comments throughout the course of this work. S. Lentz and H. Snaith made useful suggestions to improve the paper. This research was supported by an ONR graduate student fellowship to S. Gille and by National Aeronautics and Space Administration contract NAGW-1666. This is WHOI contribution 9058.

References

Barnett, T. P., Interaction of the monsoon and Pacific trade wind system at interannual time scales, I, The equatorial zone, *Mon. Weather Rev.*, *111*, 756–773, 1983.

Bottero, J. S., H. L. Bryden, D. C. Root, and J. Simpkins III, A Compilation of Observations from Moored Current Meters, XIII, *Tech. Rep. 88, Ref. 81-8*, Ore. State Univ., Corvallis, 1981.

Bretherton, F. P., R. E. Davis, and C. B. Fandry, A technique for objective analysis and design of oceanographic experiments applied to MODE-73, *Deep Sea Res.*, *23*, 559–582, 1976.

Bryden, H. L., The Southern Ocean, in *Eddies in Marine Science*, edited by A. R. Robinson, pp. 265–277, Springer-Verlag, New York, 1983.

Chelton, D. B., Statistical reliability and the seasonal cycle: Comments on "Bottom pressure measurements across the Antarctic Circumpolar Current and their relation to the wind," *Deep Sea Res., Part A*, *29*, 1381–1388, 1982.

Chelton, D. B., M. G. Schlax, D. L. Witter, and J. G. Richman, Geosat altimeter observations of the surface circulation of the Southern Ocean, *J. Geophys. Res.*, *95*, 17,877–17,903, 1990.

Davis, R. E., Predictability of sea surface temperature and sea level pressure anomalies over the North Pacific Ocean, *J. Phys. Oceanogr.*, *6*, 249–266, 1976.

Ferraz-Mello, S., Estimation of periods from unequally spaced observations, *Astron. J.*, *86*, 619–624, 1981.

Gill, A. E., and P. P. Niiler, The theory of the seasonal variability in the ocean, *Deep Sea Res.*, *20*, 141–177, 1973.

Gille, S. T., Dynamics of the Antarctic Circumpolar Current: Evidence for Topographic Effects from Altimeter Data and Numerical Model Output, Ph.D. thesis, Mass. Inst. of Technol./Woods Hole Oceanogr. Inst. Joint Program, Cambridge and Woods Hole, Mass., 1995.

Gille, S. T., Mean sea surface height of the Antarctic Circumpolar Current from Geosat data: Method and application, *J. Geophys. Res.*, *99*, 18,255–18,273, 1994.

Graham, N. E., J. Michaelsen, and T. P. Barnett, An investigation of the El Niño-Southern Osciallation cycle with statistical models, 1, Predictor field characteristics, *J. Geophys. Res.*, *92*, 14,251–14,270, 1987.

Inoue, M., Modal decomposition of the low-frequency currents and baroclinic instability at Drake Passage, *J. Phys. Oceangr.*, *15*, 1157–1181, 1985.

Jacobs, G. A., G. H. Born, M. E. Parke, and P. Allen, The global structure of the annual and semiannual sea surface height variability from Geosat altimeter data, *J. Geophys. Res.*, *97*, 17,813–17,828, 1992.

Johnson, G. C., and H. L. Bryden, On the size of the Antarctic Circumpolar Current, *Deep Sea Res., Part A*, *36*, 39–53, 1989.

Kelly, K. A., Comment on "Empirical orthogonal function analysis of advanced very high resolution radiometer surface temperature patterns in Santa Barbara Channel" by G. S. E. Lagerloef and R. L. Bernstein, *J. Geophys. Res.*, *93*, 15,753–15,754, 1988.

Large, W. G., and H. van Loon, Large scale, low frequency variability of the 1979 FGGE surface buoy drifts and winds over the Southern Hemisphere, *J. Phys. Oceanogr.*, *19*, 216–232, 1989.

Lutjeharms, J. R. E., and D. J. Baker Jr., A statistical analysis of the meso-scale dynamics of the Southern Ocean, *Deep Sea Res.*, *27A*, 145–159, 1980.

Marshall, J., D. Olbers, H. Ross, and D. Wolf-Gladrow, Potential vorticity constraints on the dynamics and hydrography of the Southern Ocean, *J. Phys. Oceanogr.*, *23*, 465–487, 1993.

Mestas-Nuñez, A. M., D. B. Chelton, M. H. Freilich, and J. G. Richman, An evaluation of ECMWF-based climatological wind stress fields, *J. Phys. Oceanogr.*, *24*, 1532–1549, 1994.

Minster, J. F., and M. C. Gennero, High-frequency variability of western boundary currents using ERS 1 3-day altimeter data, *J. Geophys. Res.*, *100*, 22,603–22,612, 1995.

Nowlin, W. D., Jr., and J. M. Klinck, The physics of the Antarctic Circumpolar Current, *Rev. Geophys.*, *24*, 469–491, 1986.

Park, Y.-H., and L. Gambéroni, Large-scale circulation in the South Indian Ocean from Topex/Poseidon altimetry (abstract), *Eos Trans. AGU*, *75*(44), Fall Meet. Suppl., 53, 1994.

Patterson, S. L., Surface circulation and kinetic energy distributions in the Southern Hemisphere oceans from FGGE drifting buoys, *J. Phys. Oceanogr.*, *15*, 865–884, 1985.

Preisendorfer, R. W., *Principal Component Analysis in Meteorology and Oceanography*, 425 pp., Elsevier, New York, 1988.

Sciremammano, F., Jr., R. D. Pillsbury, W. D. Nowlin Jr., and T. Whitworth III, Spatial scales of temperature and flow in Drake Passage, *J. Geophys. Res.*, *85*, 4015–4028, 1980.

Shum, C. K., R. A. Wender, D. T. Sandwell, B. H. Zhang, R. S. Nerem, and B. D. Tapley, Variations of global mesoscale eddy energy observed from Geosat, *J. Geophys. Res.*, *95*, 17,865–17,876, 1990.

Stammer, D., and C. W. Böning, Mesoscale variability in the Atlantic Ocean from Geosat altimetry and WOCE high-resolution numerical modeling, *J. Phys. Oceanogr.*, *22*, 732–752, 1992.

Stammer, D., and C. Wunsch, Preliminary assessment of the accuracy and precision of TOPEX/POSEIDON altimeter data with respect to the large-scale ocean circulation, *J. Geophys. Res.*, *99*, 24,584–24,604, 1994.

van Loon, H., Half-yearly oscillations in the Drake Passage, *Deep Sea Res.*, *19*, 525–527, 1972.

Vassie, I., R. Spencer, D. Smith, and G. Hargreaves, BPR measurements of the ACC across the Drake Passage, *Intl. WOCE Newsl.*, *16*, pp. 30–31, WOCE Intl. Proj. Office, Wormley, UK, 1994a.

Vassie, J. M., A. J. Harrison, P. L. Woodworth, S. A. Harangazo, and M. J. Smithson, On the temporal variability of the transport between Amsterdam and Kerguelen Islands, *J. Geophys. Res.*, *99*, 937–949, 1994b.

Weare, B. C., and J. S. Nasstrom, Examples of extended empirical orthogonal function analyses, *Mon. Weather Rev.*, *110*, 481–485, 1982.

Wearn, R. B., Jr., and D. J. Baker Jr., Bottom pressure measurements across the Antarctic Circumpolar Current and their relation to the wind, *Deep Sea Res., Part A*, *27A*, 875–888, 1980.

Whitworth, T., III, and R. G. Peterson, Volume transport of the Antarctic Circumpolar Current from bottom pressure measurements, *J. Phys. Oceanogr.*, *15*, 810–816, 1985.

Whitworth, T., III, and D. Pillsbury, Monitoring pressure difference across the ACC, *Intl. WOCE Newsl.*, *16*, pp. 28–29, WOCE Intl. Proj. Office, Wormley, UK, 1994.

Whitworth, T., III, R. D. Pillsbury, M. I. Moore, and R. F. Weiss, Observations of the Antarctic Circumpolar Current and deep boundary current in the Southwest Atlantic, *J. Geophys. Res.*, *96*, 15,105–15,118, 1991.

Wunsch, C., Sampling characteristics of satellite orbits, *J. Atmos. Oceanic Technol.*, *6*, 891–907, 1989.

Sarah T. Gille, Scripps Institution of Oceanography, 9500 Gilman Drive, La Jolla, CA 92093-0230. (e-mail: sgille@ucsd.edu)

Kathryn A. Kelly, Department of Physical Oceanography, MS21, Woods Hole Oceanographic Institution, 360 Woods Hole Road, Woods Hole, MA 02543-1541.

(Received July 25, 1995; revised December 18, 1995; accepted January 11, 1996.)